

Received February 16, 2022, accepted March 7, 2022, date of publication March 16, 2022, date of current version March 23, 2022.

Digital Object Identifier 10.1109/ACCESS.2022.3159968

Online Filter Parameters Estimation in a Double Conversion UPS System for Real-Time Model Predictive Control Performance Optimization

TIAGO J. L. OLIVEIRA^{1,2}, (Student Member, IEEE),
LUÍS M. A. CASEIRO², (Member, IEEE), ANDRÉ M. S. MENDES^{1,2}, (Member, IEEE),
SÉRGIO M. A. CRUZ^{1,2}, (Senior Member, IEEE),
AND MARINA S. PERDIGÃO^{2,3}, (Member, IEEE)

¹DEEC, University of Coimbra, 3030-290 Coimbra, Portugal

²Instituto de Telecomunicações, 3030-290 Coimbra, Portugal

³Polytechnic Institute of Coimbra, 3030-199 Coimbra, Portugal

Corresponding author: André M. S. Mendes (amsmdes@ieee.org)

This work was supported in part by the Programa Operacional Temático Competitividade e Internacionalização—Fundo Europeu de Desenvolvimento Regional (FEDER) under Project SACT-45-2017-POCI-01-0145-FEDER-029112—PTDC/EEI-EEE/29112/2017, and in part by the Foundation for Science and Technology (FCT)—Orçamento de Estado (OE). The work of Tiago J. L. Oliveira was supported in part by the FCT, and in part by the European Social Fund (ESF) under Scholarship 2020.04803.BD.

ABSTRACT Uninterruptible Power Supplies (UPS) represent the key technology to continuously feed and protect a wide range of critical applications in electric power systems. Due to their continuous operation, UPS components degrade over time, including their filtering elements, leading to decreased filtering capabilities. With these deviations, UPS performance is typically reduced. Moreover, if filter parameter deviations are not considered in the control system, performance degradation can be further increased and the critical load can be seriously compromised. This is especially important with Model Predictive Control (MPC), which heavily relies on system parameters accuracy. Thus, control performance optimization using estimated filter parameters in UPS systems can be extremely important. Nevertheless, this has not yet been covered in the literature for UPS systems. In light of these facts, this paper proposes a new mechanism that, by using online estimated filter parameters, optimizes the performance of an MPC strategy, in a UPS system. In the scope of this optimization mechanism, an estimation method that enables parameter identification and control optimization not only in balanced but also in highly unbalanced filter conditions (rarely studied in the literature) is proposed. Experimental results demonstrate the accuracy of the proposed estimators and the effectiveness of the proposed control performance optimization mechanism. Under severe filter parameter variations, the proposed performance optimization scheme enabled to reduce the degradation (caused by filter variation) of the grid current and load voltage THD by 29.41 % and 91.60 %, respectively. Furthermore, the degradation of the RMS load voltage value was also significantly reduced by 97.89 %.

INDEX TERMS Model predictive control, online inductance and capacitance estimation, power quality, real-time control performance optimization, uninterruptible power supply.

I. INTRODUCTION

From the different types of existing power quality improvement systems, Uninterruptible Power Supplies (UPS) represent the most common solution to protect critical loads in electric power systems. Unlike other commonly used power quality improvement solutions such as the static synchronous

compensator (STATCOM) and unified power flow controller (UPFC), UPS systems have energy storage capability. This enables UPS systems to not only guarantee certain power quality requirements in the load during small grid disturbances (which may also be achieved by several power quality improvement systems) but also to uninterruptedly supply a critical load even during grid outages (not supported by any other power quality improvement solution). From the different types of UPS systems, the double conversion UPS

The associate editor coordinating the review of this manuscript and approving it for publication was Vitor Monteiro¹.

system represents the topology that provides the highest level of protection to a given critical load since it fully isolates the load from the grid disturbances [1], [2]. In this type of UPS, the grid-side converter is usually connected to the mains through an inductive filter that allows the UPS to draw currents with low harmonic distortion. As for the load-side converter, it is usually connected to an LC filter to enable the generation of high-quality voltage waveforms to the critical load [3].

UPS filter parameters are typically selected to guarantee current and voltage filtering without compromising the dynamic response of the system. Usually, it is assumed that these parameters do not change over their lifetime, and consequently constant parameter values are defined in UPS controllers [3]. Nevertheless, since UPS systems have a continuous operation, their filter elements can significantly degrade over time, thus affecting the filtering capabilities and UPS performance. Besides the normal aging of components, filter degradation can also be caused by abnormal component stress such as that caused by grid disturbances, overload conditions, faults in other components or by transient phenomena. Moreover, the UPS performance can be significantly compromised if the parameters considered by UPS controllers are not accurate. Thus, online estimation of UPS filter parameters for continuous real-time control optimization is extremely important. Nevertheless, this topic has not been studied yet in the literature for UPS systems.

Several strategies have been proposed for filter parameters estimation in different power electronics applications. These strategies can be broadly grouped into two main categories [4], [5]: offline and online estimation methods. Since offline methods may require system deactivation, they do not typically represent a suitable solution for a wide range of applications, including UPS systems. Hence, additional emphasis has been given to online estimation methods especially in grid-connected converters [6]–[9], rectifiers [10]–[13] and electrical machine drives [14]–[20] applications. In [6], an estimation method using a prediction error algorithm and two specific discrete-time models is proposed to determine the parameters of an LCL filter in a grid-connected converter. In [7], a gradient descent optimization (GDO) algorithm is proposed to estimate the LCL filter parameters of a grid-connected converter. In [8] the filter inductance of a vehicle-to-grid (V2G) inverter is estimated by calculating the dot product between the grid voltage vector and the observed grid virtual-flux vector. In [11], an estimation method based on a Model Reference Adaptive System (MRAS) approach is proposed to identify the inductances of a rectifier input filter. MRAS-based methods are also investigated in [14]–[16] and [21] to estimate the inductances of a Permanent Magnet Synchronous Motor (PMSM) and the filter parameters of an inverter LC filter, respectively. In [9], an estimation method based on the Recursive Least-Squares (RLS) algorithm is proposed to identify the filter inductances of paralleled grid-connected converters. RLS-based

estimation methods are also proposed in [10] and [19] to respectively estimate an inductive rectifier filter and the inductances of a PMSM. Parameter estimation methods based on Extended Kalman Filters (EKF) have also been widely investigated, especially for electrical machines [17], [18], [20]. Finally, in [22], the parameters of an inverter LC filter are identified by estimating the instantaneous charge transferred from the inverter to a power grid.

Parameter estimation methods based on artificial neural networks (ANN) have also been proposed [23], [24]. As reported in several studies, this type of technique has shown to be a very promising solution for parameters estimation [5], [25]. Nevertheless, a significant drawback of these methods is that they typically require an offline training stage. In addition, since in the training stage limited datasets are used, an optimal estimation performance could not be ensured for all system operating conditions. Conversely, the Adaptive Linear Neuron (ADALINE) network corresponds to a simple single-layer neural network that does not require an offline training stage, being trained online. Therefore, its potential has been shown in several works regarding not only filter parameter estimation [2], [12], [24], [26] but also current/voltage harmonic components identification [27], [28] and flux estimation in electrical machines [23], which have reported a good estimation accuracy. Furthermore, according to [5], [25], ADALINE-based parameter estimation techniques typically require lower computational burden and present faster convergence than more conventional estimation methods, including those based on EKFs [17], [18], [20] and MRAS [11], [14]–[16]. Thus, its low computational complexity and good estimation accuracy turn ADALINE into a highly promising solution to be used with control approaches that simultaneously present high computational burden and whose performance considerably depends on an accurate system model, which is precisely the case of Model Predictive Control (MPC). For these reasons, the proposed estimation strategy will be based on an ADALINE network.

MPC has proven to be a highly promising control approach for power electronics applications, including UPS systems [3], [29]. In comparison with the most commonly used control strategies, such as PI control with a modulation stage, MPC typically provides several advantages including faster dynamic response without overshoot, as demonstrated in [3], [30]. In addition, multiple objectives, system nonlinearities and constraints can be more easily integrated into the control design [29], [31]. Nevertheless, one disadvantage of this control approach is its typically high computational burden. Another limitation is related to the fact that MPC directly uses the system mathematical model to minimize an objective function. For this reason, the control performance is directly related to the accuracy of the system model. In this way, several works have been proposed to minimize this limitation by using online filter parameter estimation methods to optimize the performance of MPC in real-time [7], [8], [14], [15], [24]. Nevertheless, little investigation has been made on using ADALINE-based parameter estimation for

MPC performance optimization. Only a few works have been recently reported combining these two techniques (in PMSM drives [24], [26] and inverter [14] applications). Thus, the combination of these two methods in UPS system applications represents a contribution of this paper.

As previously described, numerous works have been proposed for parameter estimation in different applications. Despite that, only [2] proposes an estimation method to identify the filter parameters of a UPS system. Nevertheless, this study has several limitations such as: the estimated parameters are not considered in UPS controllers to optimize its performance in real-time; the estimation strategy cannot reliably estimate filter parameters in unbalanced filter conditions; no experimental validation is presented.

Another limitation of the existing studies is that, with exception of [2], [9], conventional 2-level converters are still used. Furthermore, in practically all studies, the effectiveness of the proposed methods to reliably estimate filter parameters under unbalanced filter conditions is not demonstrated. Only in [9], unbalanced cases are considered in the inductive filters of two grid-connected inverters. Unbalanced filter conditions are common and can have different causes. One of them is associated with component value tolerance: since equal filter elements (same nominal manufacturer values) typically have different real values, even when identical components are used in each phase, a balanced filter condition might not be obtained. Another reason is related to the amount of stress imposed on each filter component over time: if different components suffer different degradation (for example due to grid unbalance or other unbalanced phenomena), the filtering capabilities of each phase will diverge, causing an unbalanced filter condition. Due to these facts, reliable estimation of unbalanced filters in UPS systems is extremely important, and represents an objective of this work.

In light of these facts, this paper contains the following contributions:

- proposal of an online estimation method based on an ADALINE network to reliably estimate all filter parameters of a UPS system, not only in balanced but also in unbalanced filter conditions - rarely studied in the literature.
- proposal of a mechanism to optimize the performance of an MPC strategy, by using the estimated parameters, updated in real-time, even when the UPS operates in highly unbalanced filter conditions.
- comparative analysis that demonstrates the importance of using online filter parameter estimation methods for control performance optimization in UPS systems.

The remainder of this paper is organized as follows: in Section II the studied system and mathematical model of the double conversion UPS is presented; in Section III the proposed parameter estimation methods are described; in Section IV the adopted predictive control strategy is demonstrated; in Section V experimental results are presented and Section VI presents the main conclusions.

II. STUDIED SYSTEM AND MATHEMATICAL MODEL

As represented in Fig. 1, the studied UPS system has a grid-side converter (GSC) and a load-side converter (LSC) which are connected to a double-capacitor DC bus. The measured signals required for UPS controllers are represented in red and the additional measured signals for parameter estimation are represented in green. These additional sensors are necessary to ensure a reliable estimation under unbalanced filter conditions, as will be explained in Section III. For the sake of simplicity, the DC-DC converter and battery bank are not considered in this study since the majority of the time the power grid is available and the load power flows through the GSC and LSC. These two converters are 3-Level Neutral Point Clamped (3LNPC) converters, each one with three converter legs. Each leg is associated to a phase X : in the GSC $X \in \{R, S, T\}$ whereas in the LSC $X \in \{A, B, C\}$. Each converter leg contains 4 IGBTs with anti-parallel diodes and 2 clamping diodes. In each phase there are three distinct switching states $S_X \in \{1, 0, -1\}$ which, by neglecting any voltage drop across the semiconductors, lead to three distinct pole voltage values $v_{XM} \in \{v_{C1}, 0, -v_{C2}\}$, respectively. The pole voltage is the voltage generated between the AC terminal of phase X and the middle point M of DC bus. For each converter, there are 27 possible switching states. Typically, the semiconductor forward voltages are neglected in the control scheme. Thus, in this work, they are not considered as well in the UPS controllers. Nevertheless, a constant forward voltage in the semiconductors (V_{FW}) is considered in the estimators, to maximize their performance. For example, the phase R pole voltage (v_{RM}) considered in the estimators when $i_R > 0$ and $S_R = 1$ is given by $v_{RM} = v_{c1} + 2 \cdot V_{FW}$, where the term $2 \cdot V_{FW}$ represents the forward voltage in the two anti-parallel diodes of the upper two power switches. The pole voltages in the other GSC phases and LSC are obtained analogously.

The UPS filter at the grid-side is an inductive filter, whereas at the load-side a second-order LC filter is adopted. The Equivalent Series Resistance (ESR) of all capacitors is neglected in the UPS controllers since it is very small, thus being not represented in Fig. 1. Nevertheless, as described in Section III, this value is considered in the proposed capacitance estimator. In the following, the mathematical model of the GSC and LSC is described.

A. GRID-SIDE CONVERTER

From Fig. 1 the following voltage equation can be written for the GSC

$$v_{sX} = L_{Gx} \frac{di_X}{dt} + R_{Gx} i_X + v_{XM} - v_{OM}. \quad (1)$$

In this equation, the term v_{sX} represents the grid phase voltage (calculated from the measured phase-to-phase voltages) and the term i_X denotes the current in phase X of the GSC (flowing through the phase X filter inductor), with $X \in \{R, S, T\}$. The term v_{OM} is the converter Common Mode

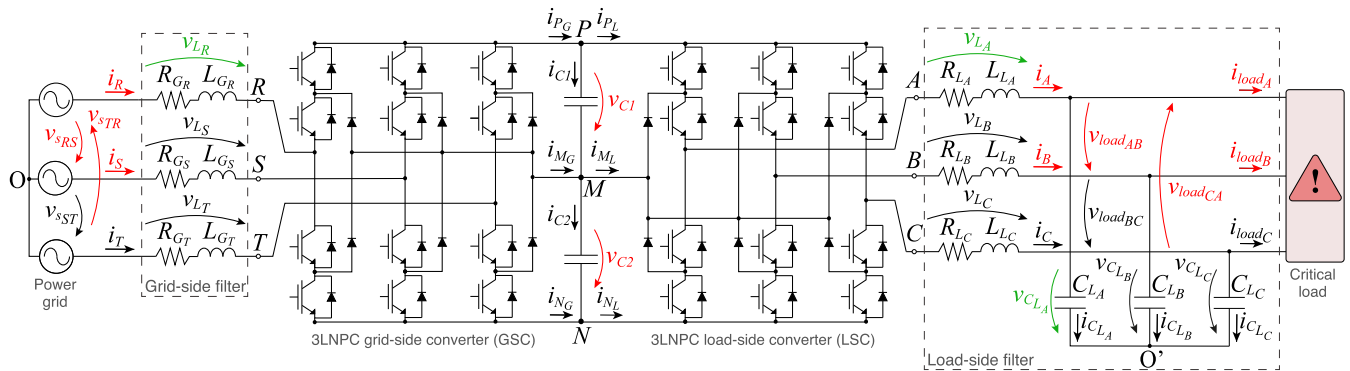


FIGURE 1. UPS system representation.

Voltage (CMV), in which the point O corresponds to the grid neutral point.

The grid-side current dynamics can be obtained from (1) and is given by

$$\frac{di_X}{dt} = \frac{v_{SX}}{L_{GX}} - \frac{R_{GX}}{L_{GX}}i_X - \frac{v_{XM}}{L_{GX}} + \frac{v_{OM}}{L_{GX}}. \quad (2)$$

The dynamics of the DC bus capacitor voltages, is given by

$$\frac{dv_{C1}}{dt} = \frac{1}{C_1}i_{C1} \quad \frac{dv_{C2}}{dt} = \frac{1}{C_2}i_{C2}. \quad (3)$$

In these two equations, the currents in capacitors C_1 and C_2 are calculated through the equations $i_{C1} = i_{PG} - i_{PL}$ and $i_{C2} = i_{NL} - i_{NG}$. In turn, the terms i_{PG} and i_{NG} are the currents supplied to the DC bus by the GSC and i_{PL} and i_{NL} are the currents drawn by the LSC. The first two terms are given by

$$\begin{cases} i_{PG} = i_R (S_R = 1) + i_S (S_S = 1) + i_T (S_T = 1) \\ i_{NG} = i_R (S_R = -1) + i_S (S_S = -1) + i_T (S_T = -1) \end{cases} \quad (4)$$

where the term $(S_X = s)$ is 1 if S_X has value s or equals 0, otherwise. The currents i_{PL} and i_{NL} are obtained analogously.

B. LOAD-SIDE CONVERTER

The equations regarding the LSC are now presented. From Fig. 1 the following voltage equation is obtained

$$v_{load_X} = -L_{LX} \frac{di_X}{dt} - R_{LX}i_X + v_{XM} - v_{O'M}, \quad (5)$$

where v_{load_X} is the load phase voltage, with $X \in \{A, B, C\}$. This term also corresponds to the voltage applied to the filter capacitor connected to phase X . Hence, this voltage is hereafter denoted as $v_{C_{LX}}$. The current i_X denotes the LSC phase X current (that flows through the respective load-side filter inductor). Finally, the terms $v_{O'M}$ and v_{XM} denote the LSC CMV (O' denotes the fictitious load neutral point) and the converter pole voltage, respectively.

As for the LSC inductor current, the following equation can also be written

$$i_X = i_{load_X} + i_{C_{LX}} = i_{load_X} + C_{LX} \frac{dv_{C_{LX}}}{dt}. \quad (6)$$

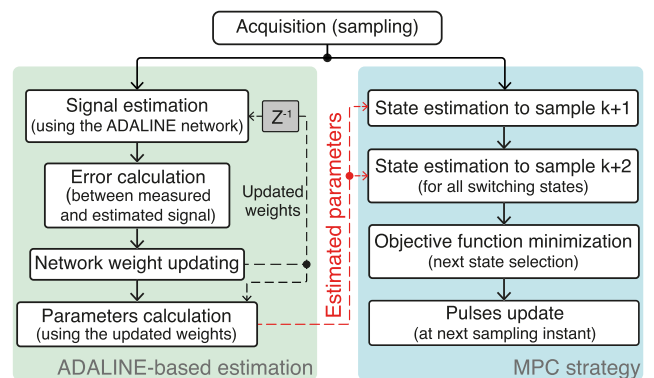


FIGURE 2. Overall representation of the proposed MPC performance optimization mechanism.

Hence, from (5) and (6) the current and voltage dynamics are given by

$$\frac{di_X}{dt} = -\frac{1}{L_{LX}}v_{C_{LX}} - \frac{R_{LX}}{L_{LX}}i_X + \frac{v_{XM}}{L_{LX}} - \frac{v_{O'M}}{L_{LX}} \quad (7)$$

$$\frac{dv_{C_{LX}}}{dt} = \frac{1}{C_{LX}}i_X - \frac{1}{C_{LX}}i_{load_X}. \quad (8)$$

III. PROPOSED PARAMETER ESTIMATION METHODS

The proposed inductance and capacitance estimation methods are described next. The principles of these two methods are similar and based on the strategies proposed in [2], [12]. Fig. 2 demonstrates the main stages of the estimation process. Each parameter estimator uses an ADALINE network (which is mathematically represented by a linear function) to estimate an output signal, by combining a set of input variables with a set of adaptive weights. The estimated signal is then compared with the respective measured signal (current or voltage) and the resulting error is used as the input of a weight adaptive function. This function adjusts the weights of the network, in order to minimize the error between the measured and estimated signal in the next iteration. In steady-state, these weights should converge to approximately

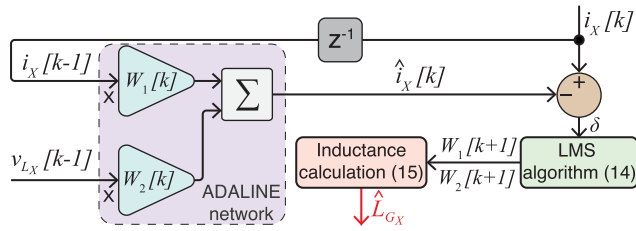


FIGURE 3. Detailed representation of the phase X grid-side filter inductance estimation process (similar for the load-side filter inductance and capacitance estimation).

constant values. Finally, the filter parameters are calculated from these recursively updated weights. As demonstrated in Fig. 2, the estimated parameters are then considered by the MPC strategy, which will be described in Section IV. Similarly to [2], [12], in this paper, the ADALINE network structures are directly defined from the system dynamics equations and not from a trial and error design approach.

In the inductance estimators, the inductor current is estimated and compared with the measured current value. In the capacitance estimators, the estimation process is quite similar, only the capacitor voltage is estimated and compared with the measured voltage, instead of current. To estimate all filter parameters, each filter component has an independent estimator. In the following, the inductance and capacitance estimation process is thoroughly described for the grid-side and load-side UPS filters.

A. GRID-SIDE FILTER INDUCTANCE ESTIMATOR

The detailed scheme regarding grid-side inductance estimation is shown in Fig. 3. As demonstrated by this figure, to estimate the inductance, the respective inductor current needs to be estimated (using the ADALINE network). In this way, by using the forward Euler approach, from (2) the following equation is obtained

$$i_x[k] = A \cdot i_x[k - 1] + B \cdot v_{Lx}[k - 1]. \quad (9)$$

In this equation, the terms $i_x[k - 1]$ and $v_{Lx}[k - 1]$ represent the inductor current and voltage at sample $k - 1$. The inductor voltage can be obtained as

$$v_{Lx}[k - 1] = v_{sx}[k - 1] - v_{xM}[k - 1] + v_{oM}[k - 1]. \quad (10)$$

In (9), the coefficients A and B are given by

$$A = 1 - \frac{T_s \cdot R_{Gx}}{L_{Gx}}, \quad (11)$$

$$B = \frac{T_s}{L_{Gx}}, \quad (12)$$

where T_s denotes the sampling period.

Based on (9), a similar equation is adapted for an ADALINE network, to estimate the inductor current (in sample k), as demonstrated in Fig. 3. This equation is given by

$$\hat{i}_x[k] = W_1 \cdot i_x[k - 1] + W_2 \cdot v_{Lx}[k - 1], \quad (13)$$

where W_1 and W_2 are the adaptive weights of the ADALINE network. Similarly to [2], [12], these weights are adjusted in every sampling period (the same as the MPC strategy), through the following iterative Least-Mean Squares (LMS) algorithm:

$$\begin{bmatrix} W_1 \\ W_2 \end{bmatrix} [k + 1] = \begin{bmatrix} W_1 \\ W_2 \end{bmatrix} [k] + \frac{\eta \cdot \delta \cdot \mathbf{X}[k - 1]}{1 + \mathbf{X}^T[k - 1] \cdot \mathbf{X}[k - 1]}. \quad (14)$$

By constantly adjusting the weights, the error between the current estimated using (13) and the measured value is minimized. This iterative LMS algorithm is equal for all estimators. In (14), η denotes the estimator learning rate and δ represents the error between the estimated and measured signal (inductor current in case of inductance estimation, as shown in Fig. 3). The term \mathbf{X} denotes the estimator input vector which is given by the measured inductor current and voltage. By comparing (9) with (13), it is clear that the minimization of the error between these currents (real and estimated) implies that the weights W_1 and W_2 converge to the value of coefficients A and B , respectively. Therefore, the estimated inductance can be obtained using an equation analogous to (12):

$$\hat{L}_{Gx} = \frac{T_s}{W_2} \approx \frac{T_s}{B}. \quad (15)$$

Even though the inductor voltage is not directly measured, it is critical for the estimation. Thus, it must be calculated. Usually, the inductor voltage is obtained from (10), which means the converter CMV needs to be known. Typically, it is assumed that this term only depends on the generated pole voltages, so in the case of the GSC, this term would be given by

$$v_{oM} = (v_{RM} + v_{SM} + v_{TM})/3. \quad (16)$$

However, this approach is only valid when each filter phase has the same inductance value. In case of an unbalance, it was observed that the converter CMV also depends on the filter parameters. Thus, by using (16), the inductor voltages are incorrectly obtained which leads to an unreliable estimation, as will be demonstrated in Section V. To overcome this interdependency, the voltage of one inductor is measured. This voltage is directly used in the respective inductance estimator, using (13), and it is also necessary to calculate the other inductor voltages. Thus, since in this work the phase R inductor voltage is measured (as shown in Fig. 1), this voltage is directly used on phase R inductance estimator. On the other hand, the inductor voltages v_{Ls} and v_{LT} are calculated using phase-to-phase system voltages and the measured inductor voltage v_{LR} :

$$v_{Ls} = v_{LR} + v_{RM} - v_{SM} - v_{sRS}, \quad (17)$$

$$v_{LT} = v_{LR} + v_{RM} - v_{TM} + v_{sTR}, \quad (18)$$

in which all terms are sampled at instant $k - 1$. This eliminates the dependency from the CMV and therefore allows a correct estimation under unbalanced filter conditions.

B. LOAD-SIDE FILTER INDUCTANCE ESTIMATOR

The load-side filter inductance estimation is performed using a similar methodology. Hence, considering a forward Euler approach discretization of (7) the following equation is obtained

$$i_X[k] = A \cdot i_X[k-1] + B \cdot v_{LX}[k-1]. \quad (19)$$

In this equation, the terms $i_X[k-1]$ and $v_{LX}[k-1]$ correspond to the inductor current and voltage at sample $k-1$, respectively. The coefficients A and B are given by

$$A = 1 - \frac{T_s \cdot R_{LX}}{L_{LX}}, \quad (20)$$

$$B = \frac{T_s}{L_{LX}}. \quad (21)$$

Similarly, the load-side filter inductor current estimated by the respective ADALINE network, is given by

$$\hat{i}_X[k] = W_1 \cdot i_X[k-1] + W_2 \cdot v_{LX}[k-1], \quad (22)$$

where W_1 and W_2 represent the respective estimator weights.

As in the grid-side filter case, an interdependency between the converter CMV and inductance parameters also exists in unbalanced conditions. To overcome this dependency, one load-side filter inductor voltage must also be measured. Thus, as shown in Fig. 1, the phase A inductor voltage is measured. This voltage is directly used in the phase A inductance estimator and in the calculation of v_{LB} and v_{LC} :

$$v_{LB} = v_{LA} + v_{AM} - v_{BM} - v_{loadAB}, \quad (23)$$

$$v_{LC} = v_{LA} + v_{AM} - v_{CM} + v_{loadCA}, \quad (24)$$

in which all terms are sampled at instant $k-1$.

Once again, using the error between the estimated inductor current and the real current value, the adaptive weights W_1 and W_2 are updated every control cycle using the iterative LMS algorithm, according to (14). In steady-state, W_1 and W_2 will converge to the values of coefficients A and B , respectively. Thus, from (21), the estimated phase X load-side filter inductance will be given by

$$\hat{L}_{LX} = \frac{T_s}{W_2}. \quad (25)$$

C. LOAD-SIDE FILTER CAPACITANCE ESTIMATOR

To estimate the load-side filter capacitances, the capacitor voltages must be estimated first. In this way, considering the capacitor ESR value, (8) is written in discrete form as

$$v_{C_{LX}}[k] = A \cdot i_{C_{LX}}[k] + B \cdot i_{C_{LX}}[k-1] + v_{C_{LX}}[k-1], \quad (26)$$

where $i_{C_{LX}}$ and $v_{C_{LX}}$ correspond to the capacitor current and voltage, respectively. The coefficients A and B are given by

$$A = ESR_X, \quad (27)$$

$$B = \frac{T_s}{C_{LX}} - A. \quad (28)$$

By rearranging (28), the following equation is obtained:

$$C_{LX} = \frac{T_s}{A+B}. \quad (29)$$

An equation analogous to (26) is used to estimate the load-side filter capacitor voltages, using the respective ADALINE network:

$$\hat{v}_{C_{LX}}[k] = W_1 \cdot i_{C_{LX}}[k] + W_2 \cdot i_{C_{LX}}[k-1] + v_{C_{LX}}[k-1], \quad (30)$$

The capacitor current $i_{C_{LX}}$ is not directly measured to avoid using additional sensors. Instead, this current is given by $i_X - i_{loadX}$. As for the capacitor voltages, in the adopted control technique only the line-to-line voltages are measured. Nevertheless, since the capacitors are star-connected, to ensure that each capacitor voltage is correctly obtained even in neutral-shift conditions, the phase A capacitor voltage is also measured, as shown in Fig. 1. This voltage is directly used in the estimation of phase A capacitor voltage using (30) and allows a direct calculation of the capacitor voltage in the other phases, using

$$v_{C_{LB}} = v_{C_{LA}} - v_{loadAB} \quad (31)$$

$$v_{C_{LC}} = v_{C_{LA}} + v_{loadCA}, \quad (32)$$

The estimated capacitor voltages obtained with (30) are compared to those measured (or calculated) at instant k , and the obtained error is used to adjust the weights W_1 and W_2 using (14). Finally, similarly to (29), the recursively updated weights are used to estimate the phase X capacitance:

$$\hat{C}_{LX} = \frac{T_s}{W_1 + W_2}. \quad (33)$$

IV. CONTROL SYSTEM

In this paper, the used control strategy is based on the MPC technique proposed in [3]. The main control steps are represented in Fig. 2. As shown in that figure, a delay of one control sampling period is considered between the sampling and converter switching state update. Hence, after measurements, the control variables are predicted to instant $k+1$. To achieve that, a forward Euler approach is used in the system mathematical model discretization. Next, for each converter, the control variables are evaluated for instant $k+2$, considering all possible converter switching states. As demonstrated in Fig. 2, both $k+1$ and $k+2$ predictions are performed using the estimated filter parameters, to optimize the control performance in real-time. Finally, after the prediction to instant $k+2$, the switching state that minimizes the converter cost function is selected and applied at instant $k+1$, after which a new control cycle starts.

The adopted control strategy relies on a cooperative principle. This means that the LSC switching state is the first to be selected. Thus, this control action is taken by only considering its effect on the UPS. However, to choose the control action for the GSC, the switching state already selected for the LSC is considered in the GSC controller [3]. In the following, the LSC and GSC controllers are presented.

A. LOAD-SIDE CONVERTER

The LSC controller must ensure two objectives: generation of a high-quality load-voltage waveform and the balancing of the two DC bus capacitor voltages. In the adopted control strategy, the three-phase variables are controlled in an $\alpha\beta$ reference frame. Therefore, to compute the $\alpha\beta$ components of current/voltage, the estimated phase parameters must also be converted to their equivalent values in the $\alpha\beta$ reference frame. To achieve that for the load-side filter inductances, (5) is written in matrix form as

$$\begin{bmatrix} v_{loadA} \\ v_{loadB} \\ v_{loadC} \end{bmatrix} = -\mathbf{L}_L \begin{bmatrix} \frac{di_A}{dt} \\ \frac{di_B}{dt} \\ \frac{di_C}{dt} \end{bmatrix} - \mathbf{R}_L \begin{bmatrix} i_A \\ i_B \\ i_C \end{bmatrix} + \begin{bmatrix} v_{AM} \\ v_{BM} \\ v_{CM} \end{bmatrix} - \begin{bmatrix} v_{O'M} \\ v_{O'M} \\ v_{O'M} \end{bmatrix}. \quad (34)$$

In this equation \mathbf{L}_L and \mathbf{R}_L are the grid-side filter resistance and inductance matrixes, which are given by

$$\mathbf{L}_L = \begin{bmatrix} L_{LA} & 0 & 0 \\ 0 & L_{LB} & 0 \\ 0 & 0 & L_{LC} \end{bmatrix} \quad (35)$$

$$\mathbf{R}_L = \begin{bmatrix} R_{LA} & 0 & 0 \\ 0 & R_{LB} & 0 \\ 0 & 0 & R_{LC} \end{bmatrix}. \quad (36)$$

By manipulating (34) using the Clarke (\mathbf{C}) and inverse Clarke (\mathbf{C}^{-1}) transformation matrixes, (34) is rewritten as

$$\begin{bmatrix} v_{load\alpha} \\ v_{load\beta} \\ v_{load0} \end{bmatrix} = -\mathbf{L}_{L\alpha\beta0} \begin{bmatrix} \frac{di_{L\alpha}}{dt} \\ \frac{di_{L\beta}}{dt} \\ \frac{di_{L0}}{dt} \end{bmatrix} - \mathbf{R}_{L\alpha\beta0} \begin{bmatrix} i_{L\alpha} \\ i_{L\beta} \\ i_{L0} \end{bmatrix} + \begin{bmatrix} v_{L\alpha} \\ v_{L\beta} \\ v_{L0} \end{bmatrix} - \begin{bmatrix} 0 \\ 0 \\ v_{O'M} \end{bmatrix} \quad (37)$$

where $\mathbf{L}_{L\alpha\beta0}$ represents $\mathbf{C} \cdot \mathbf{L}_L \cdot \mathbf{C}^{-1}$ and contains the equivalent inductances in the $\alpha\beta$ reference frame

$$\mathbf{L}_{L\alpha\beta0} = \mathbf{C} \cdot \mathbf{L}_L \cdot \mathbf{C}^{-1} = \begin{bmatrix} L_{L\alpha} & 0 & 0 \\ 0 & L_{L\beta} & 0 \\ 0 & 0 & L_{L0} \end{bmatrix}. \quad (38)$$

The Clarke transformation matrix \mathbf{C} is given by

$$\mathbf{C} = \begin{bmatrix} 2/3 & -1/3 & -1/3 \\ 0 & \sqrt{3}/2 & -\sqrt{3}/2 \\ 1/3 & 1/3 & 1/3 \end{bmatrix}. \quad (39)$$

The equivalent $\alpha\beta$ load-side filter capacitances are also obtained from the estimated phase parameters. These values are necessary not only to generate the LSC current references

but also to predict them. To achieve that, (6) is written in matrix form:

$$\begin{bmatrix} i_A \\ i_B \\ i_C \end{bmatrix} = \begin{bmatrix} i_{loadA} \\ i_{loadB} \\ i_{loadC} \end{bmatrix} + \mathbf{C}_L \begin{bmatrix} \frac{dv_{loadA}}{dt} \\ \frac{dv_{loadB}}{dt} \\ \frac{dv_{loadC}}{dt} \end{bmatrix}. \quad (40)$$

Then, similarly to the LSC inductances transformation, by manipulating (40) and using \mathbf{C} and \mathbf{C}^{-1} , the following equation is obtained

$$\begin{bmatrix} i_{L\alpha} \\ i_{L\beta} \\ i_{L0} \end{bmatrix} = \begin{bmatrix} i_{load\alpha} \\ i_{load\beta} \\ i_{load0} \end{bmatrix} + \mathbf{C}_{L\alpha\beta0} \begin{bmatrix} \frac{dv_{load\alpha}}{dt} \\ \frac{dv_{load\beta}}{dt} \\ \frac{dv_{load0}}{dt} \end{bmatrix}, \quad (41)$$

where the $\alpha\beta$ capacitance values are calculated as

$$\mathbf{C}_{L\alpha\beta0} = \mathbf{C} \cdot \mathbf{C}_L \cdot \mathbf{C}^{-1} = \begin{bmatrix} C_{L\alpha} & 0 & 0 \\ 0 & C_{L\beta} & 0 \\ 0 & 0 & C_{L0} \end{bmatrix} \quad (42)$$

For each converter control objective, a partial cost function is defined. In the adopted strategy the load voltage is controlled by controlling the LSC current. Thus, the partial cost function regarding this objective is given by

$$g_{iL} = (i_{L\alpha}^* [k + 2] - i_{L\alpha}^p [k + 2])^2 + (i_{L\beta}^* [k + 2] - i_{L\beta}^p [k + 2])^2, \quad (43)$$

where $i_{L\alpha}^* [k + 2]$ and $i_{L\beta}^* [k + 2]$ denote the LSC current references in $\alpha\beta$ reference frame, whereas $i_{L\alpha}^p [k + 2]$ and $i_{L\beta}^p [k + 2]$ represent the predicted currents.

For the second objective (DC bus capacitor voltage balancing), the partial cost function is given by

$$g_{balL} = |v_{C1}^p [k + 2] - v_{C2}^p [k + 2]|^2, \quad (44)$$

where $v_{C1}^p [k + 2]$ and $v_{C2}^p [k + 2]$ denote the predicted voltages of each DC bus capacitor for instant $k + 2$.

These partial functions are combined in a global cost function, which is evaluated every control cycle for all possible converter switching states. Hence, the LSC cost function is given by

$$G_{LSC} = g_{iL} \cdot W_{iL} + g_{balL} \cdot W_{balL}, \quad (45)$$

where W_{iL} and W_{balL} represent the weighting factors, which are used to define the importance of each objective and provide magnitude correction between control variables.

B. GRID-SIDE CONVERTER

The GSC must ensure that the currents drawn from the grid have low harmonic distortion and contribute to the balancing of the DC bus capacitors voltage. Similarly to the LSC, the GSC currents are controlled in an $\alpha\beta$ reference frame.

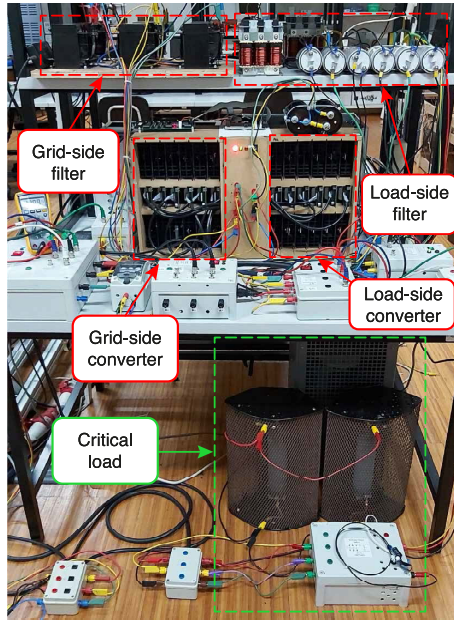


FIGURE 4. Experimental prototype.

Likewise, the equivalent $\alpha\beta$ inductance values need to be obtained from the estimated phase inductances. This conversion can be achieved in a similar way as the load-side filter inductance transformation. In this case, (1) is written in matrix form and manipulated using the Clarke transformation matrix. Then, the $\alpha\beta$ grid-side filter components are obtained analogously to (38).

For the GSC, the global cost function is given by

$$G_{GSC} = g_{i_g} \cdot W_{i_g} + g_{bal_g} \cdot W_{bal_g}, \quad (46)$$

where g_{i_g} and g_{bal_g} denote the partial cost functions regarding the GSC current reference tracking (in $\alpha\beta$) and DC bus capacitor voltage balancing. These two functions are obtained analogously to (43) and (44), respectively.

V. RESULTS AND DISCUSSION

The proposed estimators and UPS controllers were developed in *Matlab/Simulink* environment and executed in a *dSpace MicroLabBox* platform, which is also used for data acquisition at the same sampling rate ($60 \mu\text{s}$). Fig. 4 shows the main experimental setup components such as UPS converters and filtering elements. The main electrical, control and estimation parameters are shown in Table 1.

By using an autotransformer, the RMS grid line-to-line voltage was set to 120 V. Regarding the control parameters, voltage references of 220 V and 120 V were defined for the DC bus and RMS line-to-line load voltages, respectively. The DC bus uses two capacitors with a capacitance of 7 mF each. A set of experiments were made to select the minimum sampling period, with which all estimation and control algorithms can be executed without microprocessor overrun occurring. From these tests, a sampling period of $60 \mu\text{s}$ was defined. After some preliminary tests, it was also observed

TABLE 1. Main electrical, control and estimation parameters.

| Parameter | Value |
|----------------------------------------------|------------------------------------------------------------------|
| RMS grid line voltage | 120 V |
| Grid voltage frequency | 50 Hz |
| RMS load line voltage reference | 120 V |
| Load voltage frequency reference | 50 Hz |
| DC bus voltage reference | 220 V |
| DC bus capacitors capacitance | 7 mF |
| MPC weights W_{i_L}, W_{i_G} | 1 |
| MPC weights W_{bal_L}, W_{bal_G} | 0.3 |
| Control and estim. sampling period (T_s) | $60 \mu\text{s}$ |
| Semiconductor voltage drop (V_{FW}) | 1.9 V |
| Estimators learning rate (η) | 10^{-5} |
| Load | $3 \sim \text{rect.} \rightarrow 33.3 \Omega // 141 \mu\text{F}$ |

TABLE 2. Filter parameter values obtained with the LCR meter.

| Grid-side filter inductance (mH) | | | |
|------------------------------------------------|----------|----------|----------|
| | L_{GR} | L_{GS} | L_{GT} |
| Normal value | 10.42 | 10.47 | 10.56 |
| Reduced value | 5.13 | 5.18 | 5.23 |
| Load-side filter inductance (mH) | | | |
| | L_{LA} | L_{LB} | L_{LC} |
| Normal value | 2.05 | 2.05 | 2.04 |
| Reduced value | 1.01 | 1.02 | 1.01 |
| Load-side filter capacitance (μF) | | | |
| | C_{LA} | C_{LB} | C_{LC} |
| Normal value | 119.2 | 118.9 | 118.6 |
| Reduced value | 59.88 | 59.42 | 59.51 |

that the converter semiconductors present a forward voltage of roughly 1.9 V. Hence, the compensation term V_{FW} (defined in Section II) was adjusted to that value. Since the degradation of filter components is typically slow (which does not mean that significant deviations cannot be created overtime), small learning rate values are generally selected in these applications. This guarantees a stable filter parameter estimation which is fundamental for UPS controllers, without affecting the estimation accuracy. Hence, after a set of empirical tests, it was found that with a learning rate of 10^{-5} , the proposed estimators provide stable and accurate parameter estimations. Furthermore, with low learning rate values, the estimation has a relatively slow response, which enables to “filter out” most of the effect created by noise. Thus, the estimation reacts mostly to the “average” error and ignores instantaneous spikes. In addition, to further decrease the interference of switching in estimation, the switching states are altered only after the ADC conversion is complete. In the presented tests, the UPS supplies a highly non-linear load that consists of a 3-phase rectifier feeding a parallel RC circuit ($R = 33.3 \Omega$ and $C = 141 \mu\text{F}$).

Throughout the conducted experimental tests, two different values were used for each filter parameter, as shown in Table 2. From this table, it can be seen that the reduced values are roughly 50% of the normal values. All these parameters can be achieved during the tests, through the

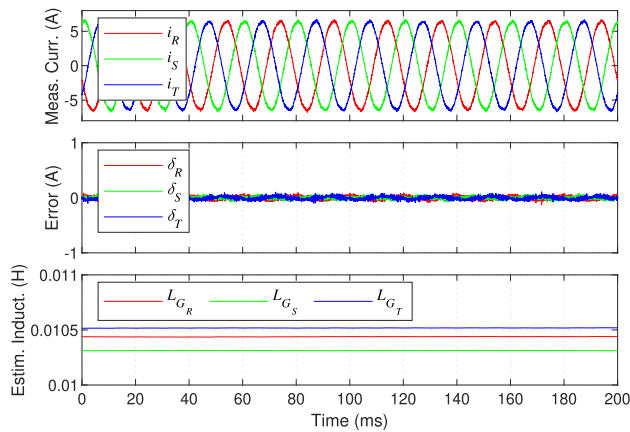


FIGURE 5. Grid-side filter inductance estimation (balanced filter condition).

connection/disconnection of two paralleled elements with the same nominal value and from the same manufacturer. For example, to reduce the filter inductance in phase X, an identical inductor is connected in parallel with the already connected inductor. On the other hand, the filter capacitance is reduced in real-time by disconnecting two paralleled capacitors. The values of Table 2 were measured using an LCR meter.

In the following, the performance of the inductance and capacitance estimators are presented considering balanced and unbalanced filter conditions. Unbalanced filters can be caused by components tolerance and/or unequal degradation in each component over time. Therefore, it is also important to evaluate the performance of the proposed estimators in these cases (significantly different parameters in each phase). After this, the importance and effectiveness of using the estimated filter parameters for real-time MPC performance optimization are demonstrated considering not only balanced but also unbalanced filter conditions.

A. ESTIMATION ACCURACY EVALUATION

1) BALANCED FILTER CONDITION

The steady-state results of the proposed estimation methods under balanced filter conditions are thoroughly represented in Figs. 5-7. These figures show the respective measured current or voltage signal, the error between the measured and estimated signal, and the estimated filter parameters. In addition, for the sake of clarity, the estimated filter parameters and respective accuracy are summarized in Table 3.

Fig. 5 demonstrates the results regarding the grid-side filter inductances estimation. From this figure, it is observed that almost sinusoidal currents flow through the grid-side filter inductors and as indicated by the small current errors, these currents are correctly estimated. Hence, in the tested conditions the phase R estimator indicates a phase R filter inductance of roughly 10.45 mH, whereas in phases S and T the estimated values are 10.30 mH and 10.51 mH, respectively. In comparison with the inductance values obtained

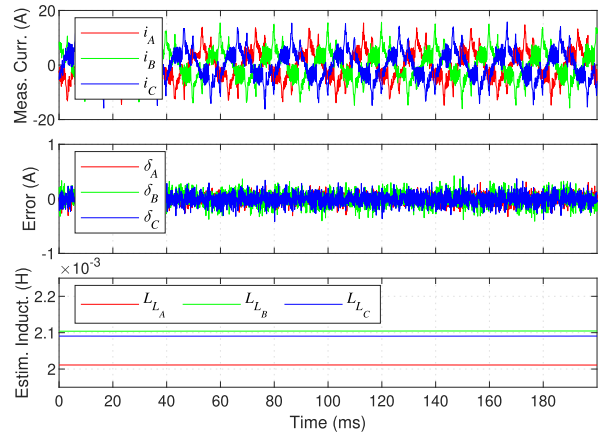


FIGURE 6. Load-side filter inductance estimation (balanced filter condition).

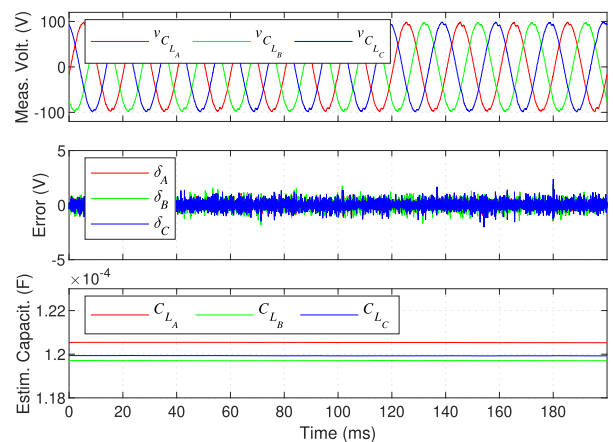


FIGURE 7. Load-side filter capacitance estimation (balanced filter condition).

with the LCR meter (Table 2), this corresponds to small estimation errors of 0.29%, 1.62% and 0.47%, respectively. These estimation deviations are mainly caused by imprecision in the sensors gain and offset definition, ADC sampling non-simultaneous with digital output updating, and delays in IGBTs activation.

Fig. 6 shows the load-side filter inductances estimation in a balanced filter condition. As shown in this figure, the converter supplies a highly non-linear load, which complicates the current estimation process. Nevertheless, the inductor currents are accurately estimated as demonstrated by the small errors in the three phases. The estimators indicate values of 2.02 mH, 2.10 mH and 2.09 mH for phases A, B and C load-side inductances, respectively. By comparing these estimated values with the LCR measurements (Table 2), small deviations of 1.46%, 2.44% and 2.45% are obtained, respectively.

The load-side filter capacitances estimation is shown in Fig. 7. This figure shows the measured capacitor voltages (phases B and C capacitor voltages are obtained using (31) and (32)) as well as the errors between the measured and

TABLE 3. Estimated parameters in balanced filter conditions.

| Grid-side filter inductance | | | |
|-----------------------------------|----------|----------|----------|
| | L_{GR} | L_{GS} | L_{GT} |
| Estimated value (mH) | 10.45 | 10.30 | 10.51 |
| Deviation from LCR (%) | 0.29 | 1.62 | 0.47 |
| Load-side filter inductance | | | |
| | L_{LA} | L_{LB} | L_{LC} |
| Estimated value (mH) | 2.02 | 2.10 | 2.09 |
| Deviation from LCR (%) | 1.46 | 2.44 | 2.45 |
| Load-side filter capacitance | | | |
| | C_{LA} | C_{LB} | C_{LC} |
| Estimated value (μF) | 120.5 | 119.7 | 119.9 |
| Deviation from LCR (%) | 1.09 | 0.67 | 1.10 |

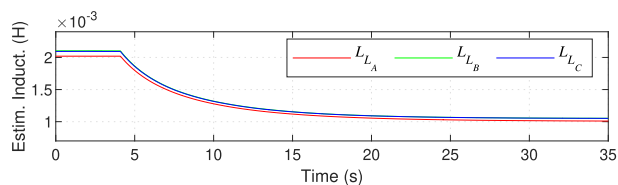


FIGURE 8. Dynamic response of the load-side filter inductance estimators (balanced variation).

estimated voltages. In this case, the parameters are also estimated with a high level of accuracy. In the tested conditions, capacitance values of 120.5 μF , 119.7 μF and 119.9 μF are estimated for phases A, B and C, respectively. When compared with the values in Table 2, these values represents low estimation errors of 1.09 %, 0.67 % and 1.10 %.

The dynamic response of the proposed estimators in balanced filter conditions is demonstrated in Fig. 8. For simplicity and to avoid redundancy, given that similar responses are obtained with the other estimators, only the dynamic response of the load-side filter inductance estimator is shown. Although filtering elements slowly degrade over time, small parameter deviations cannot be easily obtained in the laboratory. For this reason, a step variation was imposed to the filter inductance (from the normal to reduced values). Even though this sudden change does not correspond to a realistic phenomenon, it allows to demonstrate the estimators behaviour during parameter variations. Thus, as Fig. 8 shows, at $t \approx 4.10\text{ s}$ all load-side filter inductances are reduced to roughly half of their value (Table 2). After this filter variation, the estimated parameters immediately start to converge to the new inductance values, taking no more than 30 s to achieve the new steady-state condition. After reaching this new condition (reduced inductance values), the estimators provide inductance values of 1.00 mH, 1.05 mH and 1.05 mH in phases A, B and C, which in comparison with the LCR measurements represents small estimation errors of 0.99 %, 2.94 % and 3.96 %. The relatively large time window of Fig. 8 (in comparison with the current period), does not allow to clearly show the inductor currents and the error between the estimated and measured ones. For this reason, just to

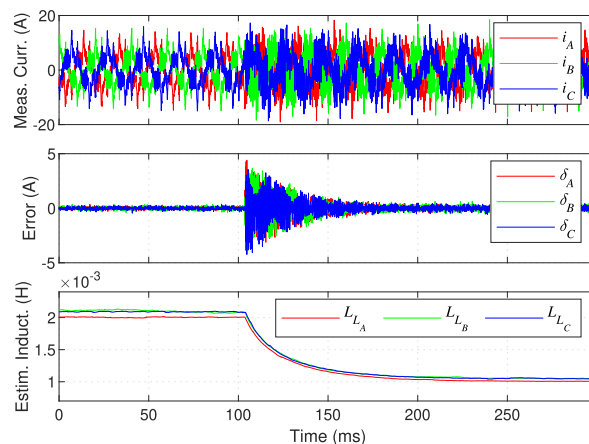


FIGURE 9. Dynamic response of the load-side filter inductance estimators (balanced variation) with a learning rate of 0.02.

better illustrate the estimators behaviour under dynamic conditions (using a shorter time window), an additional test was conducted considering the same filter variation as in Fig. 8 but with a higher learning rate being used in the estimators ($\eta = 0.02$). The results of this test are shown in Fig. 9. In this case, the filter inductances are reduced at $t \approx 103.7\text{ ms}$. After this, the errors between the measured and estimated inductor currents increase significantly to almost 5 A ($\approx 25\%$ of the peak current). This high error is mainly caused by the abrupt inductance variation which in turn immediately changes the inductor currents in a significant way. Smaller errors are therefore expected in real-world applications since considerably slower inductance variations are expected. Even so, as shown in this figure, these high current errors are effectively eliminated in all phases and the estimated inductances converge to the new steady state condition within approximately 150 ms. These results demonstrate that the proposed estimators effectively adapt to balanced filter variations.

As clearly seen in Fig. 9, the higher learning rate makes the estimator converge to the new value significantly faster. However, a considerably higher level of noise is found in the estimation in steady-state.

2) UNBALANCED FILTER CONDITION

The estimators performance under unbalanced filter conditions is now evaluated through Figs. 10-14. In addition, the estimation accuracy for the considered unbalanced cases is summarized in Table 4.

Fig. 10 shows the estimation results when the grid-side filter operates with a reduced inductance in phase B. From this figure, it can be seen that even in this unbalanced filter condition, a small current estimation error exists in the three phases. In the tested conditions, inductance values of 10.29 mH, 5.15 mH and 10.41 mH are respectively obtained for phases R, S and T, respectively. In comparison with the values obtained with the LCR meter, once again the estimation provides small errors of 1.25 %, 0.58 % and 1.42 %

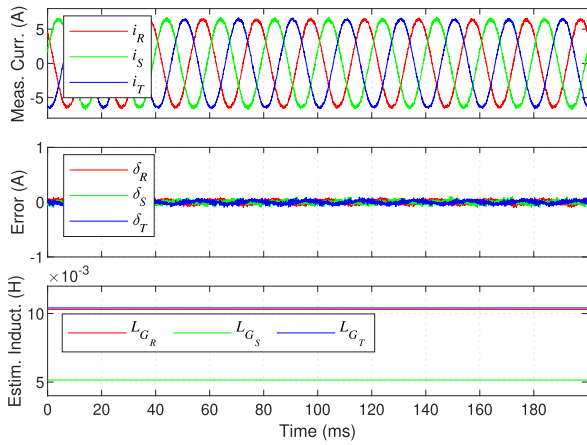


FIGURE 10. Grid-side filter inductance estimation (unbalanced condition).

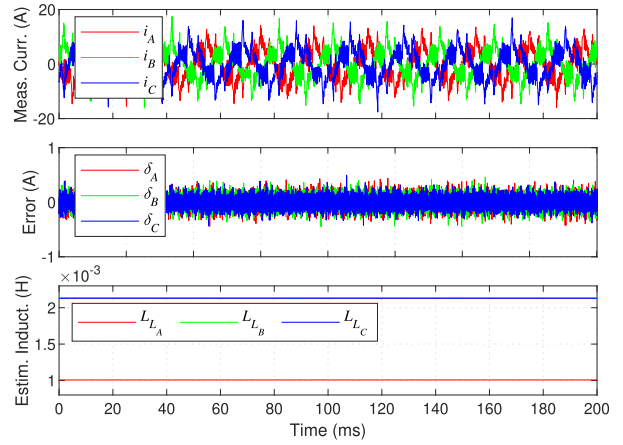


FIGURE 12. Load-side filter inductance estimation (unbalanced condition).

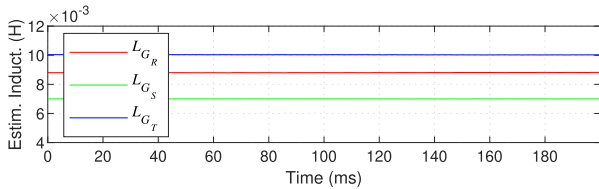


FIGURE 11. Grid-side filter inductance estimation in unbalanced case, when inductor voltages are calculated without accounting for CMV interdependency, as in [2].

for phases *R*, *S* and *T*, respectively. Fig. 11 demonstrates the importance of using an additional voltage sensor for inductance estimation in case of an unbalanced filter. In this test, the unbalanced condition is the same as that presented in Fig. 10 (phase *B* with reduced value). However, the inductor voltages were obtained through (10) and (16), using the conventional CMV equation (as used in [2]), instead of using the directly measured phase *R* inductor voltage and equations (17) and (18). As demonstrated in Fig. 11, inductance values of 8.80 mH, 7.00 mH and 10.00 mH are estimated for phases *R*, *S* and *T*, respectively. These values represent significantly large deviations of 15.55 %, 35.14 % and 5.30 %, in comparison with the values obtained with the LCR meter. This highly unreliable parameter estimation demonstrates the need of using an additional voltage sensor to correctly estimate the filter inductances in case of unbalance. This analysis is also valid for the load-side filter inductance estimation.

The results regarding the estimation of the load-side filter inductances in unbalanced filter conditions are shown in Fig. 12. In this case, the reduced inductance is used in phase *A* while phase *B* and *C* operate with the normal values. The obtained results show that even under highly unbalanced filter conditions and with a highly non-linear output current, a relatively small error is generated between each measured and estimated current signal. In this case, the estimated inductance values for phases *A*, *B* and *C* are respectively 1.00 mH, 2.14 mH and 2.13 mH, which represents small deviations

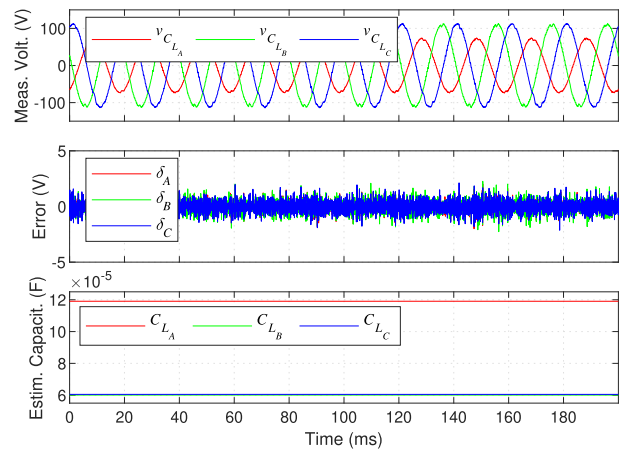


FIGURE 13. Load-side filter capacitance estimation (unbalanced condition).

TABLE 4. Estimated parameters in unbalanced filter conditions.

| Grid-side filter inductance | | | |
|------------------------------|-----------|-----------|-----------|
| | L_{G_R} | L_{G_S} | L_{G_T} |
| Estimated value (mH) | 10.29 | 5.15 | 10.41 |
| Deviation from LCR (%) | 1.25 | 0.58 | 1.42 |
| Load-side filter inductance | | | |
| | L_{L_A} | L_{L_B} | L_{L_C} |
| Estimated value (mH) | 1.00 | 2.14 | 2.13 |
| Deviation from LCR (%) | 0.99 | 4.39 | 4.41 |
| Load-side filter capacitance | | | |
| | C_{L_A} | C_{L_B} | C_{L_C} |
| Estimated value (μ F) | 119.0 | 60.1 | 60.5 |
| Deviation from LCR (%) | 0.17 | 1.14 | 1.66 |

of 0.99 %, 4.39 % and 4.41 %, relatively to the measured inductance values.

Fig. 13 demonstrates the good performance of the capacitance estimator, even under unbalanced cases. In this test, phase *A* operates with the normal capacitance whereas phases *B* and *C* operate with their respective reduced values.

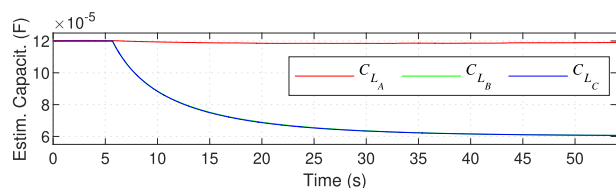


FIGURE 14. Dynamic response of the load-side filter capacitance estimators (unbalanced variation).

The filter capacitance estimators indicate capacitance values of $119.0 \mu\text{F}$ for phase A, $60.1 \mu\text{F}$ for phase B and $60.5 \mu\text{F}$ for phase C, which represents an accurate estimation, with small deviations of 0.17 %, 1.14 % and 1.66 %. In this case, as a consequence of the unbalanced condition, unbalanced capacitor voltages are also obtained. One should note that this happens because in the adopted control scheme, the line-to-line load voltages are directly controlled (instead of phase voltages). This phenomenon could be corrected by changing the control scheme. However, deep changes in the control design are out of the scope of this work.

The dynamic response of the proposed estimators when an unbalanced filter variation occurs is demonstrated in Fig. 14. As similar responses are obtained in the other estimators, only the capacitance estimation is shown here. Since small capacitance variations cannot be easily achieved in the laboratory, a step variation was also considered here. In this test, phase B and C capacitances were decreased from normal to reduced values. Once again, it is worth mentioning that this sudden parameter change does not correspond to a realistic scenario. Nevertheless, it allows to demonstrate the estimators response during an extremely unbalanced parameter variation. As demonstrated in Fig. 14, at the beginning of the test the filter operates with normal capacitance values in all phases. Then, at $t \approx 5.69 \text{ s}$ phase B and C capacitances are changed. When the filter variation occurs, the estimated capacitances start to converge to the new parameters and a new steady-state condition (presented in Fig. 13) is achieved after no more than 45 s.

These results demonstrate that the proposed estimators can effectively estimate the parameters of highly unbalanced filters and correctly adapt even to unbalanced filter variations.

3) ESTIMATION BEHAVIOUR UNDER LOAD VARIATION

The test represented in Fig. 15 aims to demonstrate the estimation behaviour when the load supplied by the UPS changes. This figure shows the power consumed by the load and all estimated parameters. In this test, the UPS system operates with the normal parameters in all filters. Two load variations are considered by changing the resistance (R) of the 3-phase rectifier + RC circuit: at $t \approx 64.97 \text{ s}$, the resistance is changed from 33.3Ω to 50Ω ; and at $t \approx 192.06 \text{ s}$, the resistance is changed again to 33.3Ω . As shown in Fig. 15, the first variation reduces the power supplied to the load by roughly 32.5 % (from 738 W to 498 W). Under this

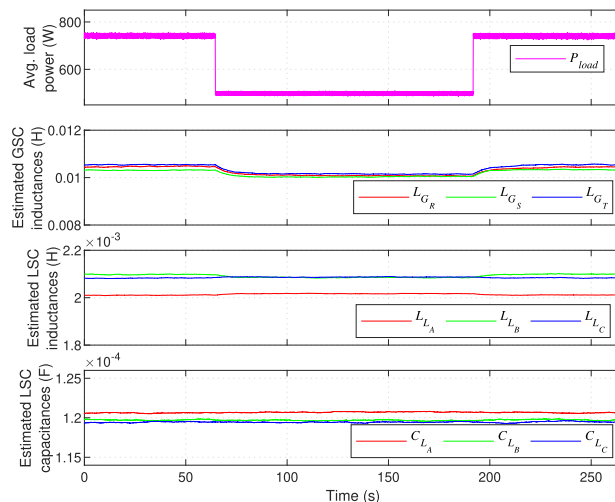


FIGURE 15. Filter parameters estimation under load variations.

TABLE 5. Phase R inductance measured with the LCR meter, at different test frequencies.

| Test frequency (Hz) | Measured inductance (mH) |
|---------------------|--------------------------|
| 100 | 10.42 |
| 1000 | 9.33 |
| 10000 | 7.12 |

considerable variation, it is observed that the estimated load-side filter inductance and capacitance values remain approximately constant. However, a higher variation is observed in the grid-side inductance estimation. In this case, as the power decreases, all estimated values also decrease. To understand this behaviour, one should note that in this filter, the current essentially consists of a predominant fundamental component (50 Hz), with a ripple that results from high frequency harmonics (imposed by switching). When the active power of the load decreases, it was observed that the fundamental component magnitude significantly decreases in comparison with the magnitude of the other high frequency harmonics. For this reason, with lower loads, the current high frequency components tend to have more effect on the real inductance value than with higher loads, decreasing its value. To illustrate this effect, Table 5 shows the phase R inductance, measured with the LCR meter at different test frequencies. It is observed that as test signal frequency increases, the inductance value decreases. This happens because as the frequency increases, the parasitic capacitance becomes more relevant, which decreases the effective inductance value. A throughout analysis of this phenomenon is out of the scope of this paper. Nevertheless, it will be considered in future research work.

Finally, to demonstrate the estimation convergence under a new load variation, the resistance is changed again to 33.3Ω (at $t \approx 192.06 \text{ s}$). After that frame, it can be observed that the estimated parameters effectively converge to the initially estimated values.

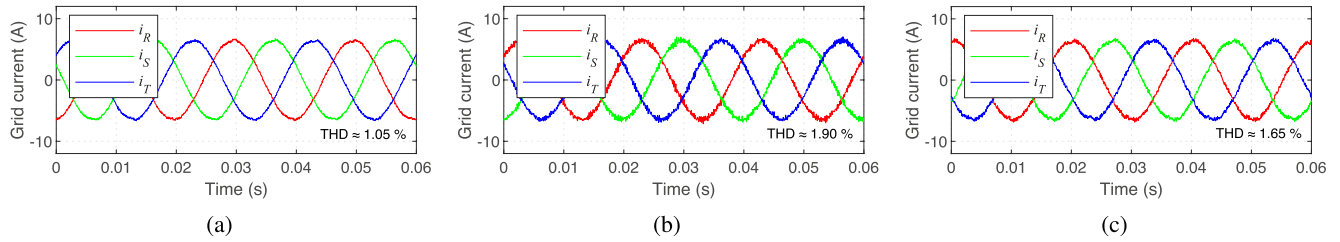


FIGURE 16. GSC controller performance evaluation in balanced filter conditions with a) normal filter inductance; b) reduced inductance, without parameter update in the controller; c) reduced inductance, with controller parameter update.

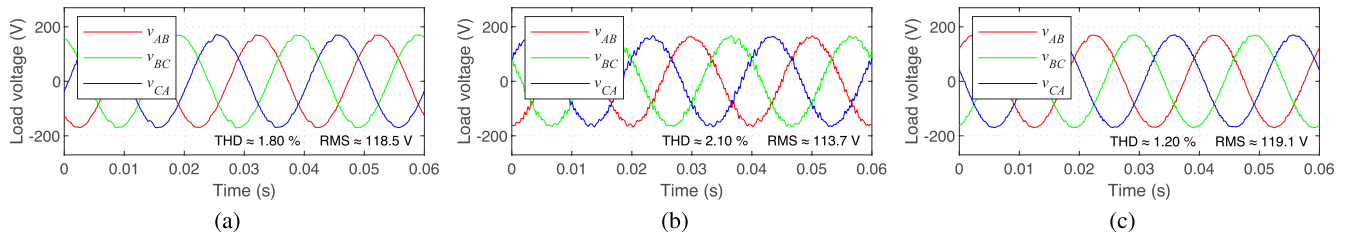


FIGURE 17. LSC controller performance evaluation in balanced filter conditions with a) normal filter inductance; b) reduced inductance, without parameter update in the controller; c) reduced inductance, with controller parameter update.

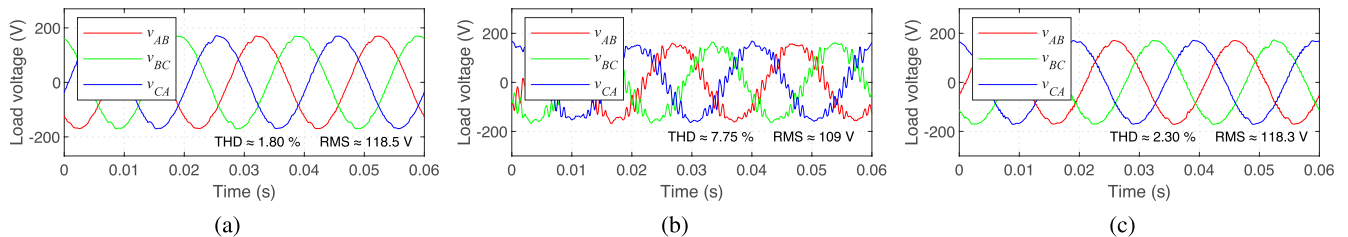


FIGURE 18. LSC controller performance evaluation in balanced filter conditions with a) normal filter capacitance; b) reduced capacitance, without parameter update in the controller; c) reduced capacitance, with controller parameter update.

B. EVALUATION OF THE PROPOSED CONTROL PERFORMANCE OPTIMIZATION MECHANISM

1) BALANCED FILTER CONDITIONS

The importance and effectiveness of using the proposed estimation methods for real-time control optimization is demonstrated in Figs. 16, 17 and 18. In these tests, only balanced filter conditions are considered. For each filtering element, the control performance is evaluated for three distinct cases: a) when the normal filter values are used (benchmark case); b) when the filter values are reduced, but the change is not considered in the controllers (no parameter update); c) when the filter values are reduced, and the new parameters are considered in the controllers (with real-time controller parameter update). A Yokogawa WT3000 power analyzer was used to obtain the current and voltage THD and RMS values. For the sake of readability, all results are summarized in Table 6.

Fig. 16(a) illustrates the case in which the grid-side filter operates with the normal inductance values. As represented in this figure, in this condition, the UPS draws currents with a THD of roughly 1.05%. Fig. 16(b) shows the grid currents when the filter inductances are reduced to approximately half

of their value, but without the estimated parameters being considered by the GSC controller. In this operating condition, it is observed that the grid currents THD significantly increases from 1.05% to 1.90%. Finally, the case in which the filter operates with the reduced values but the estimated parameters are updated in the GSC controller (in real-time) is represented in Fig. 16(c). In comparison with the case of Fig. 16(a), it is observed that the THD value increases from 1.05% to just 1.65%. This means that when the controller uses the estimated filter parameters, 29.41% of the degradation caused by the parameter variation (with no correction) is avoided. It is worth mentioning that the increase of THD in comparison with the benchmark case (1.05% to 1.65%) represents a normal behaviour since in the new condition lower inductances are used, which means lower filtering capabilities. Hence, in this latter case the current will always have higher distortion than with the regular filter values, even when highly accurate parameters are used in the controller.

Regarding the load-side filter, Fig. 17(a) demonstrates the initial operating condition in which the normal inductance values are used in the filter. In this case, the UPS generates

TABLE 6. Performance comparison under balanced filter deviations.

| | Operation with normal filter | Operat. with a reduced filter value Without update | With update |
|-------------------------------------|------------------------------|----------------------------------------------------|-------------|
| <i>Grid-side filter inductance</i> | | | |
| THD $_{i_{grid}}$ (%) | 1.05 | 1.90 | 1.65 |
| <i>Load-side filter inductance</i> | | | |
| THD $_{v_{load}}$ (%) | 1.80 | 2.10 | 1.20 |
| RMS $_{v_{load}}$ (V) | 118.5 | 113.7 | 119.1 |
| <i>Load-side filter capacitance</i> | | | |
| THD $_{v_{load}}$ (%) | 1.80 | 7.75 | 2.30 |
| RMS $_{v_{load}}$ (V) | 118.5 | 109.0 | 118.3 |

a load voltage waveform with an RMS value of 118.5 V and a THD of 1.80 %. However, as shown in Fig. 17(b), when the filter inductances are reduced to half without considering the new estimated values, the load voltage THD is increased to 2.10 % and its RMS value decreases to 113.7 V (deviation of 5.25 % from the reference value). This represents a significant reduction in UPS performance. Fig. 17(c) illustrates the case in which the filter operates with the reduced inductances and the estimated parameters are considered in the LSC controller. In this situation, a much better control performance is obtained in comparison with the results of Fig. 17(b). In this case, the THD value is reduced to 1.20 % and the RMS voltage slightly increases to 119.1 V. This means that in comparison with the case of Fig. 17(b), the THD was decreased by 42.86 %, whereas the RMS load voltage deviation (from the reference value) decreases from 5.75 % to 0.75 %. In fact, for this filtering element, the highest overall performance was observed for the case with the reduced filter (with controller parameter update), and not for the case with the normal filter. This happens mainly because a lower filter inductance value allows the LSC converter to have a faster control response. In turn, this typically improves the load voltage waveform quality when the UPS feeds highly non-linear loads (but can reduce performance with linear loads).

Finally, Fig. 18(a) represents the case in which the normal filter capacitances are used. As previously stated, in this operating condition, the UPS system ensures at the load point connection a voltage waveform with RMS and THD values of 118.5 V and 1.80 %, respectively. However, when the filter capacitances are reduced, if the estimated values are not updated in the LSC controller, the load voltage THD drastically increases to 7.75 %, as demonstrated in Fig. 18(b). In addition, its RMS value significantly decreases to 109 V, which means very weak UPS performance (deviation of 9.17 % from the reference value). Conversely, as Fig. 18(c) shows, when the estimated capacitances are considered in the LSC controller, a high UPS performance is maintained. In this case, after the capacitance variation, in comparison with the case of Fig. 18(a), the load voltage RMS slightly decreases to 118.3 V, whereas the THD value increases to just 2.30 %. This means that the proposed performance optimization mechanism enables to avoid 91.60 % and 97.89 % of the THD and RMS values degradation, caused by filter variation

(with no correction), respectively. It is worth mentioning that the results of Fig. 18(c) show a slightly lower overall performance than those from Fig. 18(a) merely because lower capacitances are used in the load-side filter (not due to estimation error). Nevertheless, as demonstrated by the results, with controller parameter update, a good overall performance is ensured even after a significant filter variation.

2) UNBALANCED FILTER CONDITIONS

The following results aim to demonstrate the effectiveness of the proposed performance optimization mechanism, especially if the UPS operates with unbalanced filters. Similarly to the analysis of Section V-B1, the control performance will be evaluated for three distinct cases: a) the benchmark case (normal parameter in all phases); b) unbalanced filter, without parameter update; c) unbalanced filter, with parameter update. Figs. 19 and 20 show the results for the load-side filter inductances and capacitances, respectively. The unbalanced conditions are the same as those presented in Section V-A2, and the main discussed results are summarized in Table 7.

Fig. 19(a) shows the benchmark case, in which similar load voltage waveforms are obtained, with an RMS and THD values of 118.5 V and 1.80 %, respectively ($v_{AB} \approx v_{BC} \approx v_{CA}$). Then, as Fig. 19(b) demonstrates, when phase A inductance is reduced by 50 %, without parameter update, the THD of the three load voltages equally increase to 2.00 %. Simultaneously, their RMS values equally decrease to 117.4 V, which represents a lower UPS performance. Finally, Fig. 19(c) shows the UPS performance when the new estimated parameters are considered in the controller. In comparison with Fig. 19(a), the THD of v_{BC} slightly increases to 1.90 % while its RMS value only decreases to 118.3 V. In turn, considering the results of Fig. 19(b), this means a degradation reduction of 50 % and 81.82 %, respectively. As for the voltages v_{AB} and v_{CA} , they actually present better THD and RMS values than in the benchmark case: the THD values are reduced to 1.50 % while the RMS values slightly increase to 118.7 V. This happens because phase A uses a lower inductance, which enables a faster response in that phase. For this reason, since the UPS supplies a non-linear load, v_{AB} and v_{CA} can be generated with superior quality than v_{BC} (which might not happen with a linear load).

As for the filter capacitors, Fig. 20(a) represents the initial case in which the normal values are used (benchmark case). When the phases B and C capacitance are reduced to a half (without control update), v_{BC} is strongly affected by the capacitance reduction in phases B and C, as shown in Fig. 20(b). In this case, its THD considerably increases to 5.75 %, while the RMS value decreases to 115.5 V. A lower performance degradation is observed in v_{AB} and v_{CA} , which present an RMS and THD values of 118 V and 4.15 %, respectively. This happens because a higher capacitance value is used in phase A (normal parameter). Finally, when the new parameter values are considered in the LSC controller, in comparison with the benchmark case, the THD of v_{BC} increases to just 2.70 %, while its RMS value slightly

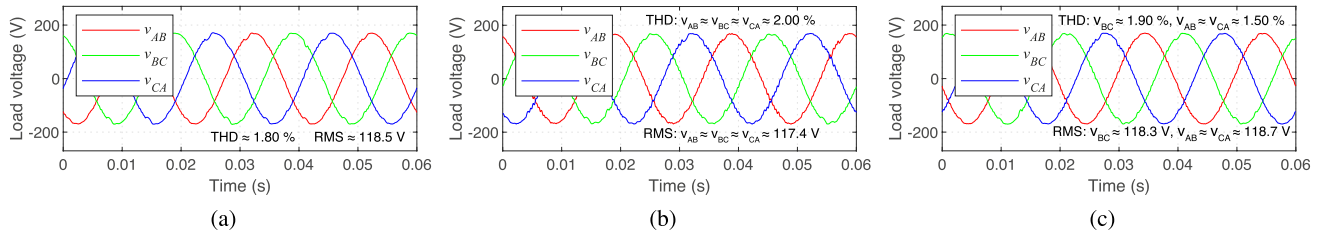


FIGURE 19. LSC controller performance evaluation operating with: a) normal filter inductance (balanced condition); b) reduced inductance in phase A, without controller parameter update; c) reduced inductance in phase A, with controller parameter update.

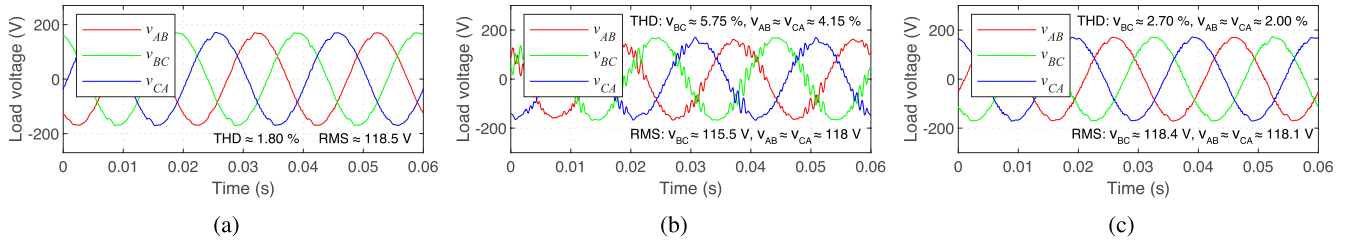


FIGURE 20. LSC controller performance evaluation operating with: a) normal filter capacitance (balanced condition); b) reduced capacitance in phases B and C, without controller parameter update; c) reduced capacitance in phases B and C, with controller parameter update.

TABLE 7. Performance comparison under unbalanced filter deviations.

| | Operation with normal filter | Operat. with a reduced filter value Without update | With update |
|--------------------------------------------------------------|------------------------------|----------------------------------------------------------|----------------------------------------------------------|
| <i>Load-side filter inductance (phase A reduced)</i> | | | |
| THD $_{v_{load}}$ (%) | 1.80 | $v_{AB} = 2.0,$ $v_{BC} = 2.0,$ $v_{CA} = 2.0$ | $v_{AB} = 1.50,$ $v_{BC} = 1.90,$ $v_{CA} = 1.50$ |
| RMS $_{v_{load}}$ (V) | 118.5 | $v_{AB} = 117.4$ $v_{BC} = 117.4$ $v_{CA} = 117.4$ | $v_{AB} = 118.7$ $v_{BC} = 118.3$ $v_{CA} = 118.7$ |
| <i>Load-side filter capacitance (phases B and C reduced)</i> | | | |
| THD $_{v_{load}}$ (%) | 1.80 | $v_{AB} = 4.15,$ $v_{BC} = 5.75,$ $v_{CA} = 4.15$ | $v_{AB} = 2.00,$ $v_{BC} = 2.70,$ $v_{CA} = 2.00$ |
| RMS $_{v_{load}}$ (V) | 118.5 | $v_{AB} = 118.0$ $v_{BC} = 115.5$ $v_{CA} = 118.0$ | $v_{AB} = 118.1$ $v_{BC} = 118.4$ $v_{CA} = 118.1$ |

decreases to 118.4 V, as illustrated in Fig. 20(c). This means that by using the estimated parameters in the UPS controller, the degradation caused by the filter variation is reduced by 77.22 % and 96.67 % regarding the THD and RMS values of v_{BC} , respectively. As for the other voltages (v_{AB} and v_{CA}), their THD values slightly increase to 2.00 % whereas the RMS values decrease to 118.1 V (degradation reduction of 91.49 % and 20.0 %, respectively). In these voltages, the THD is considerably below 2.70 % (obtained for v_{BC}) because a higher filter capacitance is used in phase A.

These results demonstrate that the proposed optimization mechanism enables to permanently optimize the performance of the adopted MPC strategy not only under balanced but also under highly unbalanced filter deviations. With this, the

UPS performance degradation caused by filter variations can be significantly avoided, as demonstrated by the presented results.

VI. CONCLUSION

In this paper, a new control performance optimization mechanism was proposed for a UPS system. The proposed mechanism uses estimated filter parameters to optimize the performance of an MPC strategy, in real-time. In the scope of this mechanism, a filter parameter estimation method is also proposed, which is based on an ADALINE network. The proposed estimators allow the estimation of all UPS filter parameters not only in balanced but also in unbalanced conditions. In turn, this has enabled the optimization of the control performance even when UPS operates with unbalanced filters. The presented experimental results have demonstrated that the proposed online estimators provide an accurate estimation of all UPS filter parameters in balanced and highly unbalanced cases. In comparison with LCR meter measurements, small maximum deviations of 2.45 % and 4.41 % were observed in the estimation for balanced and unbalanced filter conditions, respectively. The importance and effectiveness of using the proposed estimators in real-time MPC optimization were also demonstrated. It was observed that under the presence of variations in the filtering elements, by using the estimated filter parameters in the UPS controller, the degradation of the grid current and load voltage THD was reduced by 29.41 % and 91.60 %, respectively. Furthermore, the RMS load voltage value degradation was also significantly decreased by 97.89 %. These results clearly demonstrated the importance of having a control performance optimization mechanism in UPS systems.

REFERENCES

- [1] M. Aamir, K. A. Kalwar, and S. Mekhilef, "Review: Uninterruptible power supply (UPS) system," *Renew. Sustain. Energy Rev.*, vol. 58, pp. 1395–1410, May 2016.
- [2] T. J. L. Oliveira, T. M. C. Baptista, L. M. A. Caseiro, A. M. S. Mendes, M. S. Perdigão, and S. M. A. Cruz, "Online estimation of passive elements in a double conversion UPS system with no additional sensors," in *Proc. Telecoms Conf. (ConfTELE)*, Feb. 2021, pp. 1–6.
- [3] L. M. A. Caseiro, A. M. S. Mendes, and S. M. A. Cruz, "Cooperative and dynamically weighted model predictive control of a 3-level uninterruptible power supply with improved performance and dynamic response," *IEEE Trans. Ind. Electron.*, vol. 67, no. 6, pp. 4934–4945, Jun. 2020.
- [4] M. S. Rifaq and J.-W. Jung, "A comprehensive review of state-of-the-art parameter estimation techniques for permanent magnet synchronous motors in wide speed range," *IEEE Trans. Ind. Informat.*, vol. 16, no. 7, pp. 4747–4758, Jul. 2020.
- [5] Z. Q. Zhu, D. Liang, and K. Liu, "Online parameter estimation for permanent magnet synchronous machines: An overview," *IEEE Access*, vol. 9, pp. 59059–59084, 2021.
- [6] V. Pirsto, J. Kukkola, F. M. M. Rahman, and M. Hinkkanen, "Real-time identification of LCL filters employed with grid converters," *IEEE Trans. Ind. Appl.*, vol. 56, no. 5, pp. 5158–5169, Sep. 2020.
- [7] B. Long, Z. Zhu, W. Yang, K. T. Chong, J. Rodriguez, and J. M. Guerrero, "Gradient descent optimization based parameter identification for FCS-MPC control of LCL-type grid connected converter," *IEEE Trans. Ind. Electron.*, vol. 69, no. 3, pp. 2631–2643, Mar. 2022.
- [8] L. Guo, Z. Xu, N. Jin, Y. Chen, Y. Li, and Z. Dou, "An inductance on-line identification method for model predictive control of V2G inverter with enhanced robustness to grid frequency deviation," *IEEE Trans. Transp. Electrific.*, early access, Nov. 16, 2021, doi: [10.1109/TTE.2021.3128362](https://doi.org/10.1109/TTE.2021.3128362).
- [9] X. Liu, T. Liu, A. Chen, X. Xing, and C. Zhang, "Circulating current suppression for paralleled three-level T-type inverters with online inductance identification," *IEEE Trans. Ind. Appl.*, vol. 57, no. 5, pp. 5052–5062, Sep. 2021.
- [10] Y. Zhang, B. Li, and J. Liu, "Online inductance identification of a PWM rectifier under unbalanced and distorted grid voltages," *IEEE Trans. Ind. Appl.*, vol. 56, no. 4, pp. 3879–3888, Aug. 2020.
- [11] X. Liu, D. Wang, and Z. Peng, "Predictive direct power control for three-phase grid-connected converters with online parameter identification," *Int. Trans. Elect. Energy Syst.*, vol. 27, no. 1, 2017, Art. no. e02240.
- [12] A. Bechouche, D. Ould Abdeslam, H. Seddiki, and A. Rahoui, "Estimation of equivalent inductance and resistance for adaptive control of three-phase PWM rectifiers," in *Proc. 42nd Annu. Conf. IEEE Ind. Electron. Soc. (IECON)*, Oct. 2016, pp. 1336–1341.
- [13] A. Bechouche, H. Seddiki, D. O. Abdeslam, and K. Mesbah, "Adaptive AC filter parameters identification for voltage-oriented control of three-phase voltage-source rectifiers," *Int. J. Model., Identificat. Control*, vol. 24, no. 4, p. 319, 2015.
- [14] X. An, G. Liu, Q. Chen, W. Zhao, and X. Song, "Adjustable model predictive control for IPMSM drives based on online stator inductance identification," *IEEE Trans. Ind. Electron.*, vol. 69, no. 4, pp. 3368–3381, Apr. 2022.
- [15] X. An, G. Liu, Q. Chen, W. Zhao, and X. Song, "Robust predictive current control for fault-tolerant operation of five-phase PM motors based on online stator inductance identification," *IEEE Trans. Power Electron.*, vol. 36, no. 11, pp. 13162–13175, Nov. 2021.
- [16] K. Yin, L. Gao, W. Fu, and Z. Feng, "Deadbeat predictive current control of PMSM with nonlinear parameters online identification," in *Proc. IEEE 4th Int. Conf. Electron. Technol. (ICET)*, May 2021, pp. 138–142.
- [17] X. Li and R. Kennel, "General formulation of Kalman-filter-based online parameter identification methods for VSI-fed PMSM," *IEEE Trans. Ind. Electron.*, vol. 68, no. 4, pp. 2856–2864, Apr. 2021.
- [18] Z. Mynar, P. Vaclavek, and P. Blaha, "Synchronous reluctance motor parameter and state estimation using extended Kalman filter and current derivative measurement," *IEEE Trans. Ind. Electron.*, vol. 68, no. 3, pp. 1972–1981, Mar. 2021.
- [19] J. Zhang, F. Peng, Y. Huang, Y. Yao, and Z. Zhu, "Online inductance identification using PWM current ripple for position sensorless drive of high-speed SPMSM," *IEEE Trans. Ind. Electron.*, early access, Dec. 2, 2021, doi: [10.1109/TIE.2021.3130327](https://doi.org/10.1109/TIE.2021.3130327).
- [20] R. Raja, T. Sebastian, and M. Wang, "Online stator inductance estimation for permanent magnet motors using PWM excitation," *IEEE Trans. Transp. Electrific.*, vol. 5, no. 1, pp. 107–117, Mar. 2019.
- [21] S. Mukherjee, P. Shamsi, and M. Ferdowsi, "Estimation of parameters in single phase grid connected and stand-alone inverter system," in *Proc. IEEE Appl. Power Electron. Conf. Expo. (APEC)*, Mar. 2017, pp. 448–453.
- [22] V. R. Chowdhury and J. W. Kimball, "Operation of a three-phase stand-alone inverter with online parameter update by instantaneous charge transfer estimation," in *Proc. IEEE Energy Convers. Congr. Expo. (ECCE)*, Oct. 2020, pp. 2563–2568.
- [23] Z. Wang, M. Yang, L. Gao, Z. Wang, G. Zhang, H. Wang, and X. Gu, "Deadbeat predictive current control of permanent magnet synchronous motor based on variable step-size adaline neural network parameter identification," *IET Electr. Power Appl.*, vol. 14, no. 11, pp. 2007–2015, 2020.
- [24] L. Wang, G. Tan, and J. Meng, "Research on model predictive control of IPMSM based on adaline neural network parameter identification," *Energies*, vol. 12, no. 24, p. 4803, Dec. 2019.
- [25] H. Ahn, H. Park, C. Kim, and H. Lee, "A review of state-of-the-art techniques for PMSM parameter identification," *J. Electr. Eng. Technol.*, vol. 15, no. 3, pp. 1177–1187, May 2020.
- [26] A. Y. Cherif, S. E. Islam Remache, K. Barra, and P. Wira, "Adaptive model predictive control for three phase voltage source inverter using ADALINE estimator," in *Proc. 1st Global Power, Energy Commun. Conf. (GPECOM)*, Jun. 2019, pp. 164–169.
- [27] S. Janpong, K. Areerak, and K. Areerak, "Harmonic detection for shunt active power filter using ADALINE neural network," *Energies*, vol. 14, no. 14, p. 4351, Jul. 2021.
- [28] A. Tamer, L. Zellouma, M. T. Benchouia, and A. Krama, "Adaptive linear neuron control of three-phase shunt active power filter with anti-windup PI controller optimized by particle swarm optimization," *Comput. Electr. Eng.*, vol. 96, Dec. 2021, Art. no. 107471.
- [29] P. Karamanakos, E. Liegmann, T. Geyer, and R. Kennel, "Model predictive control of power electronic systems: Methods, results, and challenges," *IEEE Open J. Ind. Appl.*, vol. 1, pp. 95–114, 2020.
- [30] C. S. Lim, S. S. Lee, Y. C. C. Wong, I. U. Nutkani, and H. H. Goh, "Comparison of current control strategies based on FCS-MPC and D-PI-PWM control for actively damped VSCs with LCL-filters," *IEEE Access*, vol. 7, pp. 112410–112423, 2019.
- [31] S. Vazquez, J. Rodriguez, M. Rivera, L. G. Franquelo, and M. Norambuena, "Model predictive control for power converters and drives: Advances and trends," *IEEE Trans. Ind. Electron.*, vol. 64, no. 2, pp. 935–947, Feb. 2017.



TIAGO J. L. OLIVEIRA (Student Member, IEEE) was born in Coimbra, Portugal. He received the M.Sc. degree in electrical engineering from the University of Coimbra, Portugal, in 2019, where he is currently pursuing the Ph.D. degree in electrical engineering with the Instituto de Telecomunicações. He joined the Instituto de Telecomunicações as a Researcher, in 2019. His research interests include control, fault diagnosis, and fault-tolerant techniques for power electronics converters.



LUÍS M. A. CASEIRO (Member, IEEE) was born in Leiria, Portugal. He received the M.Sc. and Ph.D. degrees in electrical engineering from the University of Coimbra, Coimbra, Portugal, in 2012 and 2017, respectively. He is currently collaborating with the Instituto de Telecomunicações, Coimbra. His research interests include high-quality and high-reliability power electronics converters, with particular emphasis on fault diagnosis, fault tolerance, digital control, and rapid prototyping techniques.



ANDRÉ M. S. MENDES (Member, IEEE) was born in Portugal. He received the Diploma, M.Sc., and Dr.Eng. degrees in electrical engineering from the University of Coimbra, Coimbra, Portugal, in 1993, 1998, and 2005, respectively. Since 1991, he has been with the Department of Electrical and Computer Engineering, University of Coimbra, where he is currently an Assistant Professor and the Director of the Power Electronics Laboratory. He is also the Coordinator of the Power Systems

Research Group, Instituto de Telecomunicações, Coimbra. His teaching activities include electrical machines and power electronics, and his research interests include fault diagnosis and fault tolerance in electric drives and power electronic converters, wireless power transfer for electric vehicles, and power quality. He is a member of the Portuguese Engineers Association.



SÉRGIO M. A. CRUZ (Senior Member, IEEE) received the Diploma, M.Sc., and Dr.Eng. degrees in electrical engineering from the University of Coimbra, Coimbra, Portugal, in 1994, 1999, and 2004, respectively. He is with the Department of Electrical and Computer Engineering, University of Coimbra, where he is currently an Associate Professor and the Director of the Electric Machines Laboratory. His teaching and research interests include power transformers, rotating electric machines, electric drives, and power electronic converters, with special emphasis on fault diagnosis, fault tolerance, and digital control.



MARINA S. PERDIGÃO (Member, IEEE) was born in Coimbra, Portugal, in 1978. She received the M.Sc. and Ph.D. degrees in electrical engineering from the University of Coimbra, Coimbra, in 2004 and 2012, respectively. From 2006 to 2012, she conducted her Ph.D. work at the University of Coimbra in cooperation with the University of Oviedo, Oviedo, Spain. Since 2002, she has been with the Coimbra Institute of Engineering, Polytechnic Institute of Coimbra, Coimbra, first as a

Teaching Assistant and then as an Adjunct Professor, since 2012. Since 2001, she has been a Researcher with the Instituto de Telecomunicações, Coimbra. She is the coauthor of more than 50 journals and conference publications, including more than 20 publications in highly referenced journals. Her research interests include high-frequency switching converters, resonant converters, dc–dc converters, power electronics for renewable energies, IPT, inductor modelling, and computer simulation applications. She was the recipient of the Best Paper Award of the 2009 IEEE International Symposium on Industrial Electronics and was awarded by the Industrial Lighting and Display Committee of the IEEE Industry Applications Society a First Prize Paper for the technical competence displayed. She collaborates with IEEE as a transactions paper reviewer. She is also a reviewer for other journal publications.

...